Guiding Innovations: Optimizing Sheet Hydroforming of Nimonic 90 through Brown Bear Optimization and Evaporation Water Cycle Algorithms

Fakrudeen Ali Ahamed J [1]*, N.Murali [2] and Rohan.M.Vaishta [3]

[1]Mechanical & Industrial Section, College of Engineering and Technology, University of Technology and Applied Sciences- Nizwa, P.O. Box 477, Sultanate of Oman, https://orcid.org/0000-0003-1472-3560
[2]Electrical & Electronics Section, College of Engineering and Technology, University of Technology and Applied Sciences- Nizwa , P.O. Box 477, Sultanate of Oman, https://orcid.org/0000-0001-6780-7384
[3]Micro tech India, Bengaluru, India 560079

KEYWORDS

Sheet Hydroforming, Nimonic 90, Forming limit diagram, Formability, Brown bear optimization, Evaporation based water cycle algorithm.

ABSTRACT

Sheet hydroforming is a type of hydroforming in which complex designs are formed from sheet metal using high-pressure fluids. It is a viable alternative to standard stamping or deep drawing, particularly where high precision, fewer tool components, or intricate shapes are required. Optimisation techniques are among the most promising strategies for dealing with real-world situations that involve many goals and limitations. This research proposes a method for optimizing process parameters to achieve good formability in sheet hydroforming of Nimonic 90 alloy using brown bear optimisation and the evaporation water cycle algorithm. The best results achieved through optimization techniques are validated by numerical simulation and experimentally. The outcomes achieved show that brown bear optimisation predicts the best optimal process parameters in maximising deformation and good formability of nimonic 90 alloy in sheet hydroforming.

1.Introduction

Nickel, chromium, and aluminium make up the majority of the Nimonic series of nickel-based super alloys, which are critical in high-temperature applications due to their remarkable strength and wear resistance [1]. Nimonic 90, a nickel-chromium-cobalt alloy are widely used in aerospace applications due to its ultimate strength and creep resistance even exposed at high temperatures up to 1193 K. It is produced by substituting approximately 20% of nickel with cobalt. Nimonic 90 has good ductility and is commonly used in high-temperature springs [2]. Hydroforming shown in Fig. 1 is a sheet metal forming technique that use fluid pressure to form metals of complex shape and geometries [3]. It provides benefits over traditional processes like stamping, such as increase in accuracy of dimension and material utilization [4]. The complex nature of this process, which includes nonlinear material behaviour, extensive deformations, friction, and contact mechanics, demands the use of Finite Element Analysis (FEA) in design and optimisation. Engineers can save time and money by using FEA to simulate forming processes, forecast flaws like wrinkling, tearing, and springback, and optimise process parameters without requiring a lot of physical testing. The Forming Limit Diagram (FLD) is an important tool for determining the formability of sheet metals during metal forming process. It provides a graphical representation of sheet metal forming limitations under various strain conditions, enabling engineers to predict the onset of necking or fracture [5]. The initiation of localised necking under different strain conditions could be systematically shown on a strain diagram [6]. FLDs are sensitive to material properties and process parameters [7]. The Forming Limit Diagram is an important tool in sheet metal forming analysis.

***Corresponding Author:**
fakrudeen.research@gmail.com

From its experimental start to modern computer simulations, it has evolved into a complete method for evaluating formability over a wide range of materials and settings. FEA software like LsDyna, Abaqus etc., can be used to model a variety of hydroforming procedures including fluid-based and rubber-based methods. With the advent of finite element methods (FEM), numerous studies have focused on numerical simulations of FLDs. Integrating FLD into FEM codes enables for more accurate failure prediction in forming simulations [8]. Experimental validation is critical for increasing trust in FEA models for correlating projected and measured strains, thickness distributions, and spring back to achieve simulation accuracy [9] . Optimisation is a mathematical field that gives the best solutions to complex problems across different domains like engineering, arts, advertising, etc., [10]. Optimization algorithms are becoming more and more crucial as technology develops for solving practical problems and encouraging creativity in a variety of domains, including physics, engineering, machine learning, and operations research [11]. Real-world optimisation problems are naturally challenging. They have multiple objectives and dimensions. Solving such problems with deterministic techniques is sometimes quite challenging [12]. In modern manufacturing, optimization algorithms have emerged as a critical tool for increasing efficiency and quality. As computing technology and artificial intelligence evolve, these algorithms become increasingly significant in the parameter optimization of manufacturing process [13]. Optimisation algorithm approaches look at the search space to discover the most optimal/near-optimal solutions for a given problem. Nature-inspired algorithms (NIAs) have gained significant attention in recent years, drawing inspiration from diverse sources in biology, physics, and other domains [14]. These algorithms can be classified into various categories, including bio-inspired, physics-based, and social-based approaches [14] [15]. The rapid proliferation of NIAs has led to challenges in keeping track of new developments and understanding their relationships to existing metaheuristics [16]. To address this, researchers have compiled comprehensive databases and reviews of NIAs, providing insights into their applications and taxonomies [17]. However, the use of domain-specific terminology in describing these algorithms has been criticized for obscuring their underlying principles and connections to other optimization techniques [16]. Despite these challenges, NIAs continue to be widely applied in various fields, including industrial optimization and drone technology [15] [14]. Natural phenomenon-inspired optimisation algorithms have emerged as a key component of artificial intelligence, especially when it comes to resolving challenging real-world issues. Among these, the Water Cycle Algorithm (WCA) is a novel approach that draws inspiration from the natural water cycle, which includes elements like rainfall, river flow, and streams that merge into seas. The traditional WCA finds the best answers in a landscape by simulating the flow of raindrops across rivers and streams [18]. However, researchers have suggested modifications and improvements to increase its effectiveness and more closely resemble real hydrological occurrences. The Evaporation Water Cycle Algorithm based (EWCA) is one of the noteworthy innovations. The EWCA improves on the original WCA by including the evaporation process, which is critical to maintain the balance between exploration and exploitation in the search space [19]. The Brown Bear Optimisation (BBO) algorithm, a population-based metaheuristic algorithm that replicates the smart hibernation and foraging tactics of brown bears in the natural environment [20]. BBO has demonstrated competitive benefits over classical and contemporary algorithms in performance comparisons in the following areas: robustness against local minima; convergence speed; and solution accuracy [21]. Existing research lack in optimising process parameters in sheet hydroforming of

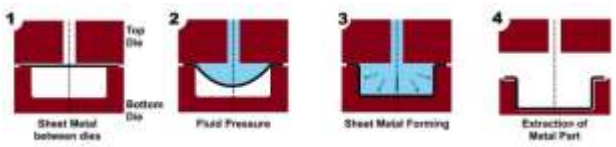

Fig. 1. Sheet Hydroforming

1.1 Research Gap and Problem Statement

The research gap analysis highlights that while numerous studies have investigated sheet hydroforming using conventional optimization techniques and established metaheuristic approaches, limited attention has been given to the application of Brown Bear Optimization (BBO) and Evaporation Water Cycle Algorithm (EWCA) for optimizing hydroforming parameters. Furthermore, the combined evaluation of these algorithms for improving formability characteristics and process performance in Nimonic 90 sheet hydroforming has not been adequately addressed in the existing literature. Based on these identified gaps, the novelty and motivation of the present study have been explicitly articulated

Nimonic alloy. To the best of the authors understanding, this is the first approach to optimise the sheet hydroforming process of a nimonic 90 using BBO and EWCA approaches. The goal of this research is to develop an improved model and method for optimising process parameters in sheet hydroforming of Nimonic 90.

- Identifying the most suitable process parameters for Nimonic 90 sheet hydroforming using nature inspired algorithms.
- Validation of optimized result using finite element analysis.
- Validation of optimized result by experimentation.

The primary contributions of this study are as follows:

Application of Emerging Metaheuristic Algorithms: The study investigates the applicability of Brown Bear Optimization (BBO) and Evaporation Water Cycle Algorithm (EWCA), which have received limited attention in sheet hydroforming optimization, particularly for Nimonic 90 alloy components. Optimization of Nimonic 90 Sheet Hydroforming Process: The work focuses on optimizing critical hydroforming process parameters to improve forming performance, addressing a material and process combination that has not been extensively explored in the existing literature. Comparative Performance Evaluation: A systematic comparison between BBO and EWCA is performed to assess their effectiveness in identifying optimal process conditions and achieving improved forming characteristics. Finite Element Validation: The optimized solutions obtained from the metaheuristic algorithms are validated through finite element analysis, demonstrating the feasibility and practical applicability of the proposed optimization framework.

The rest of the paper is grouped as follows: Section 2 discusses the material used, its properties, two nature inspired algorithms used, section 3 discusses the validated result obtained from numerical simulation and experimentation. The conclusion is discussed in section 4.

2. Material and Methodology

This section discusses material composition and properties, FEA simulation, optimization techniques used and experimental validation.

2.1 Material and its properties

The material used in this study is Nimonic 90 alloy sheet. The composition and material properties of the material is shown in Table 1 and Table 2 [22].

Tab. 1. Nimonic 90 Sheet-Material Composition [22]

Composition	%
Ni	Bal
Cr	18.649
Co	16.71
Ti	2.367
Al	1.378
Fe	0.978
Mn	0.673
Si	0.342
Cu	0.085
C	0.0819
P	0.0081
S	0.0072

Tab. 2. Nimonic 90 Sheet-Mechanical Properties [22]

Material Properties	Value
Yield strength (0.2%)	587x 10^6 Pa
Young's Modulus	105.95 x10^9 Pa
Poisson's Ratio	0.28
Maximum Tensile Strength	1271x10^6 Pa
Strain Hardening Exponent at n value	0.3038
Strength Coefficient at n value	1555.3697

2.2 Objective Function

A regression model in Response Surface Methodology (RSM) is generated in accordance with Eq. 1 to achieve maximum deformation [23] .

$$y = \alpha_0 + \sum_{i=0}^{n} \alpha_1 x_i + \sum_{i=0}^{n} \alpha_2 x_i 2 + \sum_{i=0}^{n} \sum_{j=0}^{n} \alpha_3 x_i \; xj \quad (1)$$

Where "y" refers to the output response. In addition, α_0, α_1, α_2, and α_3 indicate constant, linear, quadratic, and interaction coefficients, respectively. Furthermore, x_i and x_j are the independent variables, with E denoting the statistical error. According to Eq. 2, the center value is represented by 0 and the previously indicated factor levels were given codes ranging from -1 to +1 [23] [24].

$$x_i = \frac{x_{i-x_0}}{\Delta X} \quad (2)$$

where ΔX stands for the step change in the actual value of the variable. The objective function presented in Eq. 3, is formulated using RSM in Minitab software to maximize the deformation (De) during the hydroforming of Nimonic 90 sheet.

$$De = 8.52 + 0.3483\times Pr - 0.00044\times BHF - 14.59\times T + 0.000262\times Pr\times Pr - 0.000001\times BHF\times BHF + 7.344 \times T\times T - 0.000000\times Pr\times BHF - 0.1925\times Pr\times T + 0.00031 \times BHF\times T \quad (3)$$

2.3 Proposed methods

In this section, two methods are proposed to optimize process parameters to maximise the deformation without failure in sheet hydroforming of Nimonic 90 alloy.

2.3.1 Evaporation Water Cycle Algorithm (EWCA)

EWCA basic idea is based on the recurring process of rivers and streams emptying into the ocean. The initial population of streams is created at random, assuming that a specific location experiences rainfall. As the sea, the stream with the lowest objective function is chosen for its best value. Other stream values flow straight into rivers or the ocean. The river or the ocean absorbs the stream's water. varying streams have varying water transfer rates. If the flow of a stream provides a better solution than rivers for the maximum objective function, it can be swapped out for an accurate result. The river and the sea are likewise exchanged in this situation, according to the optimal response. Using the evaporation operator, the objective function maximization is kept from converging too soon.

The process of evaporation that occurs in the sea creates precipitation in streams and rivers. To guarantee the best possible outcome, because of the rain, new places for rivers and streams are formed near the shore. In order to verify for the maximum objective function for a specific iteration, the stream and river locations are changed. Below is a discussion of the algorithm steps.

Step 1 involves selecting the search space's initial parameters, which include M_{qw}, P_L, S_{ind}, iter and 80/20 rule. Select random population size for rivers, seas, and streams in step two.
Step 3: Determine each stream's objective function.
Step 4: Save the solutions of the random starting population in the 80/20 rule after determining the assembling space for selecting sea, rivers.
5th step: Use governing equations for determining the crowding values to determine the flow concentration of rivers and the sea.

$$Obj_n = FF_n - FF_{Mqw+1} \quad n = 1,2,3...,M_{qw} \quad (4)$$

$$NS_n = round\left\{\left|\frac{Obj_n}{\sum_{n=1}^{Nsr} Obj_n}\right| XN_{Stream_S}\right\} \quad n = 1,2,3...,M_{qw} \quad (5)$$

Step 6: The accompanying equation gives the maximum objective function by exchanging sea's locations with the stream.

$$Y_{Stream}^{t+1} = Y_{Stream}^{t} + randi * Ci * (Y_{Sea}^{t} - Y_{Stream}^{t}) \quad (6)$$

Step 7: As the matching equation, in order to achieve the maximum target function, the new position streams flow into the rivers and switch the locations of a river and a stream.

$$Y_{Stream}^{t+1} = Y_{Stream}^{t} + randi * Ci * (Y_{River}^{t} - Y_{Stream}^{t}) \quad (7)$$

Step 8: The river flows into the sea from its new place, and the sea's locations are swapped with the river's to provide the maximum objective function, as shown by the accompanying equation.

$$Y_{River}^{t+1} = Y_{River}^{t} + randi * Ci * (Y_{Sea}^{t} - Y_{River}^{t}) \quad (8)$$

The random number between 0 and 1 is called the rand.

Step 9: The rainfall process starts when the evaporation criterion, P_L, is satisfied. Calculate the objective function to find the new location with the highest value. The lower values are eliminated and the 80/20 rule is updated.

Step 10: Determine the crowding distance for each 80/20 rule and eliminate the most significant values. After choosing the new sea and river sites, make sure they meet the convergence condition; if not, move on to step 6. Table 3 shows the parameters used in EWCA.

Table 3 presents the parameter settings used for implementing the Evaporation Water Cycle Algorithm (EWCA) in the numerical simulations. These parameters control the search process, convergence behavior, and exploration capability of the algorithm. Population size: This parameter specifies the total number of candidate solutions (raindrops) generated in the search space during each iteration. A population size of 50 provides a balance between solution diversity and computational efficiency, enabling the algorithm to adequately explore the solution space while maintaining reasonable execution time. Number of waterways and oceans: This parameter determines the number of main streams and oceans used to guide the optimization process. The selected value helps organize the population into different flow groups, enhancing information exchange among candidate solutions and improving the global search capability of the algorithm. Evaporation stage variable: The evaporation parameter controls the evaporation–precipitation mechanism of EWCA, which is responsible for diversifying the search and preventing premature convergence to local optima. A value of 0.28 was selected to maintain an effective balance between exploration and exploitation during the optimization process. Maximum number of iterations: This parameter defines the stopping criterion of the algorithm. The optimization process continues for a maximum of 100 iterations, which was found sufficient to achieve stable convergence and accurate solutions for the considered problem.

Tab. 3. Parameters-EWCA

Parameters	Value
Population size (Mqw)	50
Number of waterways and oceans (PL)	4
Evaporation stage variable (Sind)	0.28
The most iterations possible (iter)	100

2.3.2 Brown Bear Optimization Algorithm (BBO)

BBO method assumes various brown bear groups within a territory are equivalent to each population's solution set. Each solution set's number of decision variables corresponds to the quantity of pedal smell marks each group produced. An issue's territory for exploration is similar to a brown bear's realm. It is same like in other population-based optimization methods. Within a territory, multiple brown bear groupings are formed at random using a predetermined amount of pedal scent markers. Different group's marks are unique characteristics that stay within the territory. The outer limits of the relevant problem's choice variables are defined by their borders. The initiation of units inside an area at random can be expressed quantitatively as follows.

Step 1: Set the population's randomly generated set to its upper and lower bounds, then assess it.

$$W_{z,x} = W_{z,x}^{min} + \lambda (W_{z,x}^{max} - W_{z,x}^{min}) \quad (9)$$

where $W_{z,x}$, zth team of brown bears' xth foot characteristic. $W_{z,x}^{min}$ and $W_{z,x}^{max}$ are the pedal markings' lowest and upper ranges, respectively. λ Is every random number dispersed equally throughout the (0 to 1) range. If a territory's total number of groups is determined by Npop and U determines each team's total number of ride indications. Thus, the group of choices W is displayed as

$$W = \begin{bmatrix} W_{x,z} & W_{x,zz} & \cdot & \cdot & W_{x,U} \\ W_{xx,z} & W_{xx,zz} & \cdot & \cdot & W_{xx,U} \\ \cdot & \cdot & \cdot & \cdot & \cdot \\ \cdot & \cdot & \cdot & \cdot & \cdot \\ W_{Npop,z} & W_{Npop,zz} & \cdot & \cdot & W_{Npop,U} \end{bmatrix} \quad (10)$$

Step 2: Evaluate fitness $f(W_i)$, if $f^{best} > f(W_i)$ then

$$f^{best} = f(W_i),\ W_K^{best} = W(i,:) \quad (11)$$

Brown bears have a unique personality and mark their pedal fragrance. It can be identified by its unique gait, cautious marching, snaking the foot against the indentations of the earth. Provide a mathematical representation of pedal trace pattern performance. Marking pedal fragrance is a behavior that only male members of the majority display. It is assumed that each group consists of one male member for simplicity's sake. The male members of each group walk in a distinct way. Traces of ride aroma produced with a typical strolling stride are expected to last for the first third of the amount of descendants, Niter.

$$W_{a,s,d}^{new} = W_{a,s,d}^{old} - \left(\theta_k * \alpha_{a,s,d} * W_{a,s,d}^{old}\right) \quad (11)$$

The modified throttle sign of the ith Brown Bear ensemble is shown in kth iteration as $W_{a,s,d}^{new}$ whereas the previous pedal mark is shown by $W_{a,s,d}^{old}$. An arbitrary integers, $\alpha_{a,s,d}$, is used to represent the sth stride milestone. Cause of the event, denoted as θd , represents the ratio of finished to ongoing iterations and increases linearly with the number of iterations. It looks like this: $\theta_d = \frac{C_{iter}}{N_{iter}}$ (12)

Step 3: Walking characteristic gait: Pedestrian scent marking behavior is primarily displayed by male members. To keep things simple, it is presumed that there is one male member in each group.

Each group's masculine participants walk in a unique way, so foot odor imprints left by them is distinct. Pedal smell markings are thought to have developed based on a distinctive walking gait up until Niter. This trait is demonstrated numerically

$$\theta_d > 0 \text{ and } d\theta_d \le \frac{C_{iter}}{N_{iter}} \quad (13)$$

where the quantity of repetitions is shown by C_{iter}.

Step 4: Revise their foot notches, employing a deliberate characteristic to increase the signs' of recognition. The following is a description of the computational framework for this attribute:

$$W_{i,j,k}^{new} = W_{i,j,k}^{old} + F_k\left(W_{j,k}^{best} - L_k * W_{j,k}^{worst}\right) \quad (14)$$

The cause of the event θ_k uses the fragrance traces on the footrest to calculate Fd. $W_{s,d}^{worst}$ and $W_{s,d}^{best}$ in every troop of brown bears.

$$F_d = \beta_{1,d} * \theta_d \quad (15)$$

A random number is used by the procedure $\beta_{1,k}$ and step length L_k to alter pedal markings that are based on the population's top and lowest pedal marks. In a group, a male brown bear makes new pedal traces with stride lengths of one or two by carefully moving forward or backward. The following is a mathematical expression for the step length L_k:

$$L_d = \text{round}(1+\beta_{2,d}) \quad (16)$$

where $\beta_{2,d}$ represents a possible value in the region that is equally dispersed [0, 1].

Step 5: Foot Twisting Characteristic: The usual foot twisting of brown bear males, particularly contribute to a firmer pedal smell marking, determines how the pedal marks in a group are updated. Other members of the group create smell maps using this feature. Successive foot traces are selected using the finest and lowest foot patterns. In a bunch of brown bears, the rate at which each male rotates his feet is represented by the following equation:

$$\omega_{y,z} = 2\pi * \theta_z * \gamma_{y,z} \quad (17)$$

In a brown bear, the angular velocity of twist is established by $\omega_{y,z}$ and $\gamma_{y,z}$, where $\omega_{y,z}$ specifies twist speed, and $\gamma_{i,z}$ is a random number between 0 and 1. This attribute is defined by the following expression.

$$W_{a,s,d}^{new} = W_{a,s,d}^{old} + \omega_{a,d} * \left(W_{s,d}^{best} - \left|W_{a,s,d}^{old}\right|\right) - \omega_{a,d} * \left(W_{s,d}^{worst} - \left|W_{a,s,d}^{old}\right|\right) \quad (18)$$

It goes without saying that the top bears group selected for this round advance to the next one.

Step 6: Sniffing activity: To communicate and regulate their movement inside their region, brown bears employ sniffing activity. To go to their group's marks, they choose pedal marks at random, leaving other traces in their wake. The following is a mathematical model of this behavior. The ath and nth bear bands' sth updated move footprints are shown in the dth repetition by $W_{a,s,d}^{new}$ and $W_{a,s,d}^{old}$, correspondingly, where a and b are distinct.

$$W_{a,s,d}^{new} = \begin{cases} W_{a,s,d}^{old} + \lambda_{i,k} * \left(W_{a,s,d}^{old} - W_{b,s,d}^{old}\right) \text{if } f\left(W_{a,s}^{old}\right) < f\left(W_{b,d}^{old}\right) \\ W_{a,s,d}^{old} + \lambda_{i,k} * \left(W_{b,s,d}^{old} - W_{a,s,d}^{old}\right) \text{if } f\left(W_{b,s}^{old}\right) < f\left(W_{a,d}^{old}\right) \end{cases} \quad (19)$$

These groups' cost value indicated $f\left(W_{a,d}^{old}\right)$ and $f\left(W_{b,d}^{old}\right)$. In the kth iteration, for the sth pedal marks, $\lambda_{i,k}$ symbolizes a random quantity between 0 and 1, which is uniformly distributed. Table 4 shows the parameters used in BBO.

Table 4 summarizes the parameter settings used in the Brown Bear Optimization (BBO) algorithm. These parameters govern the population structure, search behavior, and convergence performance of the optimization process. Number of brown bears: This parameter represents the total population of brown bears (candidate solutions) initialized in the search space. Each brown bear corresponds to a potential solution of the optimization problem. A larger population increases the diversity of solutions and enhances the exploration capability of the algorithm, while a smaller population reduces computational complexity. Number of pedal marks (DDD): The pedal marks parameter denotes the dimensionality of the optimization problem, i.e., the number of decision variables to be optimized. Each pedal mark reflects a search direction or movement dimension followed by the brown bears during the optimization process. Random number (λ\lambdaλ): This parameter is a stochastic control factor used to introduce randomness into the movement and searching behavior of the brown bears. It helps maintain diversity within the population, improves exploration of the search space, and reduces the likelihood of premature convergence to local optima. Maximum number of iterations (NiterN_{iter}Niter): This parameter specifies the termination criterion of the algorithm. The optimization process continues until the maximum number of iterations is reached. Increasing the iteration number generally improves convergence accuracy but also increases computational time

Tab. 4. Parameters-BBO

Parameters	Value
Number of brown bears (Npop)	30
Number of pedal marks (D)	3
Random number(λ)	0 to 1
Maximum number of iterations(Niter)	100

2.4 Validation

In this section, the methods of FEA and experimental validation conducted for the best optimized process parameters obtained through BBO technique are presented.

2.4.1 Finite element analysis

The current work used shell elements to represent components for FEA simulations using the Autodesk Fusion 360 software, as indicated in Fig. 2. The use of shell elements in FEA yields better results and reduces time required for computation [25].

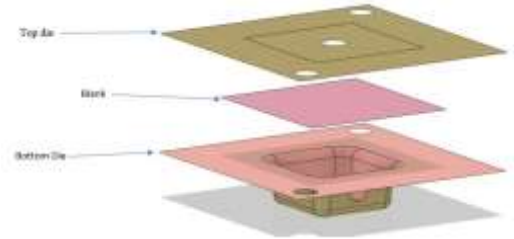

Fig. 2. Shell Elements

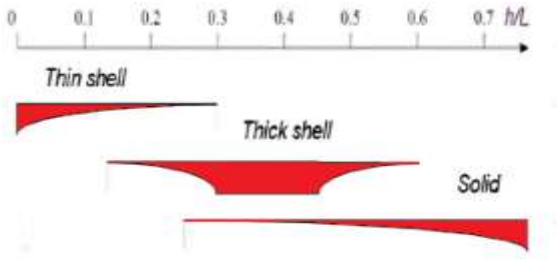

Fig. 3. H/L Chart

According to the approximation model illustrated in Fig. 3, the thin shell approximation is utilised in this model since the thickness to length ratio (h/L Chart) is within 0.3. Ansys-Mechanical is utilized for meshing in this study. With its structural, thermal, acoustic, transient, and nonlinear features, this best-in-class finite element solver improves models. Quadrilateral elements are used which generates smoother surfaces compared to triangle components, which often result in surface abnormalities [24].

Analysis is carried out in LS-Dyna. The elastic and plastic properties of the material are specified using multi-linear points. Material properties are specified using piecewise linear plasticity model. Table 2 lists the properties of the nimonic 90 sheet, which serve as input for the elastic region. The true plastic stress strain values presented in Table 5 are used as input for the plastic region. The appropriate finite element mesh nodes are subjected to boundary conditions and optimized process parameters like pressure, BHF and thickness. The analysis carried for the input parameters.

Tab. 5. True plastic stress-strain of Nimonic 90 sheet

True Plastic Strain (mm/mm)	True Plastic Stress (MPa)
0	587.00
0.0011	605.141
0.0031	621.649
0.011	651.828
0.02914	686.214
0.0544	720.61
0.07823	754.973
0.1043	789.214
0.12939	823.752
0.15341	858.273
0.20062	927.014
0.22421	961.463
0.2455	995.744
0.26861	1030.232
0.28991	1064.64
0.3115	1099.01
0.33252	1133.53
0.35441	1167.92
0.37573	1202.12
0.39812	1236.84
0.4191	1271.01

2.4.2 Experimental Validation

Experimental work was carried out to validate the optimized results. In order to achieve this, the experimental setup model shown in Fig. 4 was developed.

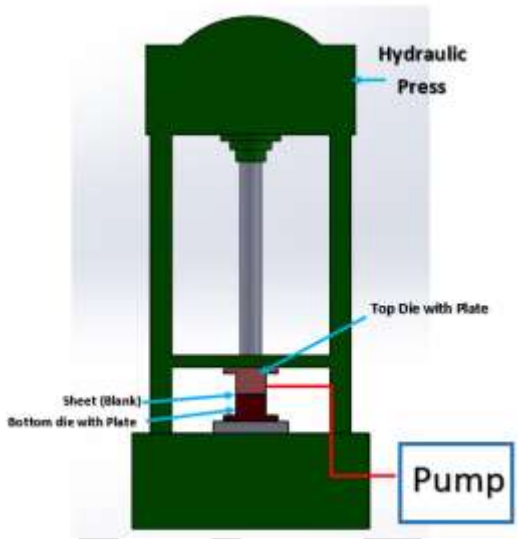

Fig. 4. Model of SHF

The nimonic 90 sheet specimen of 65 × 65 mm, as illustrated in Fig. 5, is cut and engraved using a laser engraving equipment, making small circle grids with a diameter of 2mm and a depth of 5 microns. This investigation used two dies, top and bottom dies with plates as indicated in Fig. 6 and Fig. 7. The dies were made from P20 tool steel, a material noted for its excellent resistance to deformation [26], with the dimensions stated in Table 6.

Tab. 6. Dimensions of Die and Sheet

Component	Dimension (mm)
Top Die	100 × 100
Bottom Die	100 × 100
Sheet (Blank)	65 × 65
Sheet Thickness	0.8, 1 and 1.2
Die's Cavity	38 × 38 × 20
Die corner radius	4 to 6

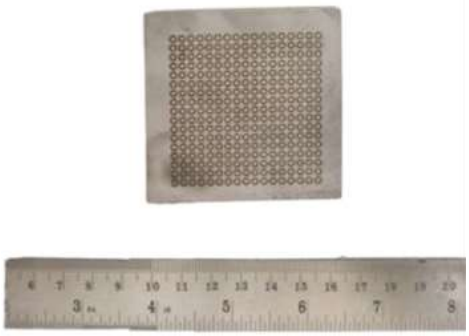

Fig. 5 Nimonic 90 specimen–Circle engraved

A 100-ton hydraulic press, as shown in Fig. 8, is used to hold the top die and provide the necessary blank holder force (BHF). The fluid pressure is applied to the top of the sheet using a 1000 bar pump.

Fig. 6. Top die with plate

Fig. 7. Bottom die with plate

Fig. 8. Experimental Setup

3. Result and Discussion

Using eqn. 3 and the lower and upper bound values of the process parameters stated in table 7, the BBO and EWCA optimisation techniques are used to optimise in order to achieve the maximum deformation (De).

Tab. 7. Process parameters and its levels

Process Parameters	Lower Level	Middle Level	Higher Level
Pressure (MPa)	30	40	50
BHF(kN)	180	200	220
Thickness (mm)	0.8	1.0	1.2

The maximum deformation during the hydroforming of a nimonic 90 sheet with the BBO approach's optimized process parameters shown in Fig. 9. The convergence is shown in Fig.10 and Fig.11 using EWCA and BBO approach. The maximum deformation for nimonic 90 sheet without failure, as determined by FEA simulation using optimized parameters obtained by the BBO method, is shown in Table 7. BBO optimisation differs by 0.03% from the maximum deformation found in FEA simulation.

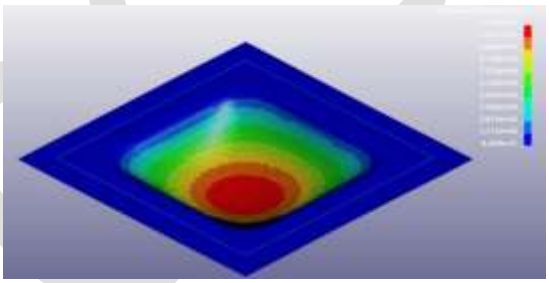

Fig. 9. FEA Simulation-Deformation-BBO Approach

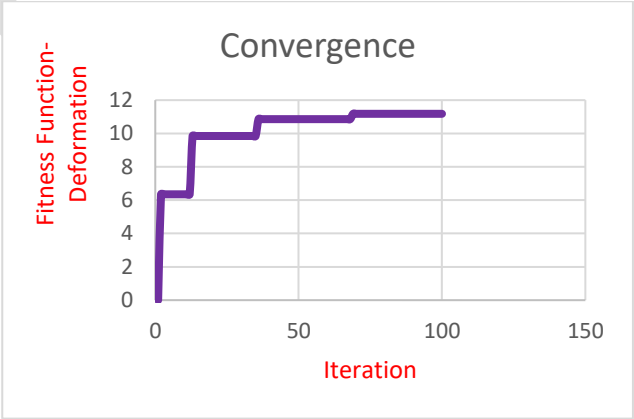

Fig. 10. Convergence-EWCA

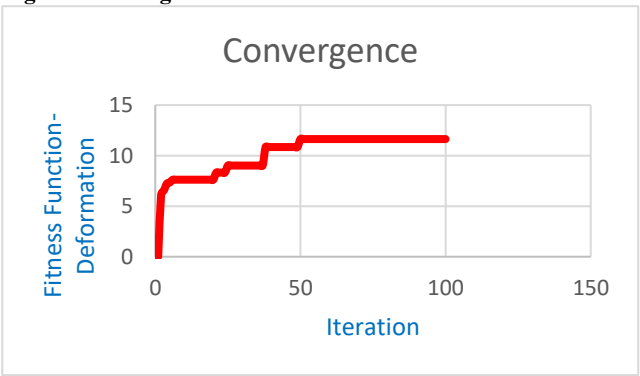

Fig. 11. Convergence-BBO

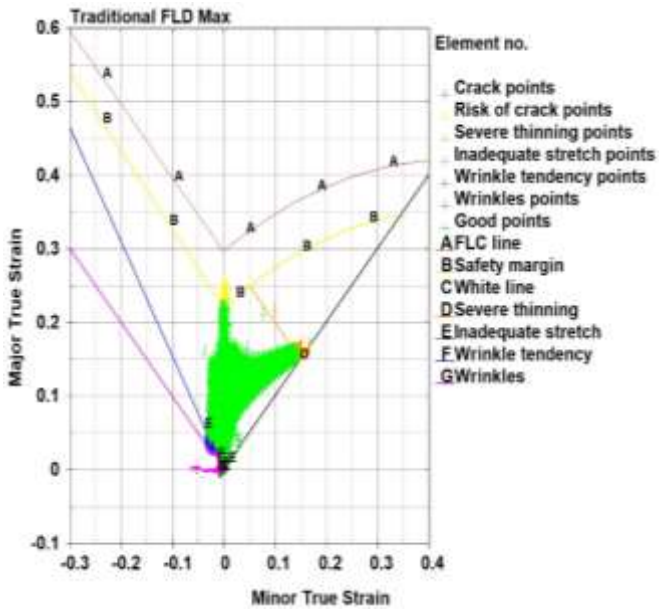

Fig. 12. Forming Limit Diagram

The FLD generated by the LSDyna with the optimized process parameters of the BBO algorithm is displayed in Fig. 12. The simulation's FLD for nimonic 90 showed no failure zone, indicating that the determined optimum process parameter values by BBO method were acceptable.

3.2 Experimental Validation

A confirmatory experiment was carried out in accordance with the approach described in section 2. The experimental validation result of the deformed nimonic sheet for the optimal process parameters generated through the BBO approach is shown in Fig. 13. The maximum deformation is obtained without failure is shown in the table. The suggested BBO approach is successful in predicting the maximum deformation is obtained without failure is shown in the table. The suggested BBO approach is successful in predicting the best parameters needed to generate the intended output response because the error percentage for both FEA and experimental validation with the optimized parameters obtained by the BBO algorithm for both nimonic 90 is less than 5% [27].

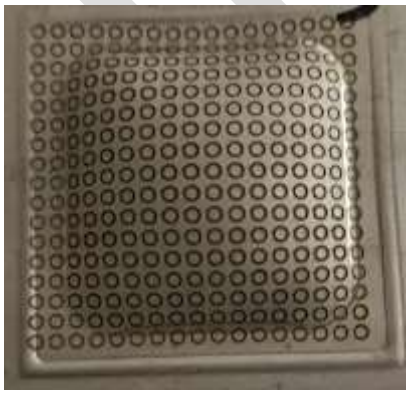

Fig. 13. Experimental Validation

Tab. 7. Process parameters and its levels

Process Parameters			BBO-Predicted Deformation (mm)	EWCA-Predicted Deformation (mm)	FEA Simulation Validation Deformation (mm)	Experimental Validation Deformation (mm)	% of error	
Pressure (MPa)	BHF (kN)	T (mm)					FEA	Experimental
49	159	0.8	11.64	11.34	11.68	11.44	0.03	1.71

4.Conclusion

In order to investigate the necessary pressure, blank holding force, and thickness reductions, a finite element simulation and experimentation for optimization of process parameters for the formability of Nimonic 90 in sheet hydroforming was carried out in this study. The following briefly summarizes the study's key findings. The introduction of fluid pressure during the sheet hydroforming process causes the sheet to stretch in the flange region, producing strains that are above the wrinkling limit curve as seen in the forming limit diagram (FLD). This condition benefits the sheet metal forming process. Finite element analysis and experimentation shows that BHF, pressure, and sheet thickness are critical parameters for preventing wrinkling during forming. The FLD for nimonic 90 sheet obtained from FEA simulation validation show no failure zones, indicating that these optimum process parameter values are acceptable. The maximum deformation obtained without failure in FEA and experimental validation are 11.68 mm and 11.44 mm respectively. The error between FEA simulation deformation and BBO optimization is 0.03%. The error between experimental deformation and BBO optimization is 1.71%. The results suggest that the BBO algorithm produces better results for optimizing the process parameters of SHF of Nimonic 90. Future study will focus on applying the same techniques to evaluate the formability of various super alloys of parts of complex geometry. The application of cutting-edge improved optimization techniques is a potential scope for machine learning approaches.

References

[1] Dubey. D, Mukherjee. R, & Singh. M. K., "*A review on tribological behavior of nickel-based Inconel superalloy*," Proc. Inst. Mech. Eng. Part J J. Eng. Tribol., Vol. 238, no. 6, 2024, PP. 706–732.

[2] Khajuria. G & Wani . M. F., "*High-Temperature Friction and Wear Studies of Nimonic 80A and Nimonic 90 Against Nimonic 75 Under Dry Sliding Conditions*," Tribol. Lett., Vol. 65, no. 3, 2017, PP. 100.

[3] G.-A. Costin, C. Afteni, I. Iacob, V. Păunoiu, and N. Baroiu, "*An Overview On Sheet Metal Hydroforming Technologies*," Ann." Dunarea Jos" Univ. Galati, Fascicle V, Technol. Mach. Build., Vol. 36, 2024, PP. 55–62.

[4] Achuthankutty. A., Ramesh.A., & Velamati. R. K., "*A 3D Non-Linear FE Model and Optimization of Cavity Die Sheet Hydroforming Process*," Metals (Basel)., Vol. 14, no. 4,2024, PP. 478.

[5] Marciniak. K. K. Z., "*Limit strains in the processes of stretch-forming sheet metal*," Int. J. Mech. Sci., 1967, PP. 609–620.

[6] Keeler. S. P., & Backhofen. W. A., "Plastic Instability and Fracture in Sheet Stretched over Rigid Punches," ASM Trans. Q., Vol. 56, no. 11, 1963, PP. 25–48.

[7] Li. B., & Nye. T. J., "*Prediction of Forming Limit Diagrams for Aluminum Alloy Sheet Using Finite Element Analysis*," in Volume 2: Computer Technology, ASMEDC, 2006, PP. 9–377.

[8] Ahamed. F. A., Chinnaiyan. J. P., & Vashishta. R. M., "*Hydroforming of nimonic 80 A sheet: a novel optimization based numerical simulation*," Int. J. Interact. Des. Manuf., 2024.

[9] Hu. H., Wang. J.F., Fan. K. T., Chen. T. Y., & Wang. S. Y., "*Development of sheet hydroforming for making an automobile fuel tank*," in Proceedings of the Institution of Mechanical Engineers, Part B: Journal of Engineering Manufacture, SAGE Publications Ltd, 2015, PP. 654–663.

[10] Singiresu S Rao., "*Engineering Optimization Theory and Practice*," John Wiley & Sons, Inc, 2020, PP. 1-56.

[11] Alridha. A. H., Abd Alsharify. F.H., & Al-Khafaji. Z., "*A Review of Optimization Techniques: Applications and Comparative Analysis*," Iraqi J. Comput. Sci. Math., Vol. 5, no. 2, 2024.

[12] Mandal. P. K., "*A review of classical methods and Nature-Inspired Algorithms (NIAs) for optimization problems*," Results Control Optim., Vol. 13, 2023, PP. 100315.

[13] Song. J., Wang. B., & Hao. X., "*Optimization Algorithms and Their Applications and Prospects in Manufacturing Engineering*," Materials (Basel)., Vol. 17, no. 16, 2024, PP. 4083-4093.

[14] Darvishpoor. S., Darvishpour. A., Escarcega. M., & Hassanalian. M., "*Nature-Inspired Algorithms from Oceans to Space: A Comprehensive Review of Heuristic and Meta-Heuristic Optimization Algorithms and Their Potential Applications in Drones*," Drones, Vol. 7, no. 7, 2023, PP. 427-437.

[15] Slowik. A., & Cpalka. K., "*Hybrid Approaches to Nature-Inspired Population-Based Intelligent Optimization for Industrial Applications*," IEEE Trans. Ind. Informatics, Vol. 18, no. 1, 2022, PP. 546–558.

[16] Lones. M.A., "*Mitigating Metaphors: A Comprehensible Guide to Recent Nature-Inspired Algorithms*," SN Comput. Sci., Vol. 1, no. 1, 2020, PP. 49-59.

[17] Tzanetos. A., Fister. I., & Dounias. G., "*A comprehensive database of Nature-Inspired Algorithms*," Data Br., Vol. 31, 2020, PP. 105792.

[18] Eskandar. H., Sadollah. A., Bahreininejad. A., & Hamdi. M.," *Water cycle algorithm – A novel metaheuristic optimization method for solving constrained engineering optimization problems*," Comput. Struct., Vol. 110–111, 2012, PP. 151–166.

[19] Hussien. A. G., Hashim. F. A., Qaddoura. R., Abualigah. L., Pop. A., "*An Enhanced Evaporation Rate Water-Cycle Algorithm for Global Optimization*," Processes, Vol. 10, no. 11, 2022, PP. 2254.

[20] Prakash. T., Singh. P. P., Singh. V. P., & Singh. S. N., "*A Novel Brown-bear Optimization Algorithm for Solving Economic Dispatch Problem*," in Advanced Control & Optimization Paradigms for Energy System Operation and Management, Vol. 199, New York: River Publishers, 2023, PP. 137–164.

[21] Chaib. L., Tadj. M., Choucha. A., El-Rifaie. A. M., & Shaheen. A. M., "*Hybrid Brown-Bear and Hippopotamus Algorithms with Fractional Order Chaos Maps for Precise Solar PV Model Parameter Estimation*," Processes, Vol. 12, no. 12, 2024, PP. 2718.

[22] Ahamed. F. A. & Chinnaiyan. P, "*Studies on Finite Element Analysis in Hydroforming of Nimonic 90 Sheet*," Mathematics, Vol. 11, no. 11, 2023, PP. 2437-2347.

[23] Khuri, A.I. & Mukhopadhyay, S. (2010), *Response surface methodology*. WIREs Comp Stat, 2: 128-149

[24] Demirel. C., Kabutey. A., Herák. D., Sedlaček. A., Mizera . Č., & Dajbych. O., "*Using Box–Behnken Design Coupled with Response Surface Methodology for Optimizing Rapeseed Oil Expression Parameters under Heating and Freezing Conditions*," Processes, Vol. 10, no. 3, 2022, PP. 480-490.

[25] Vasile. R., Racz. S. G, & Bologa. O, "*Numerical and Experimental Analysis of The Formability Of 1.4301 Austenitic Stainless Steel Sheets Using Hydroforming*," Manuf. Syst., Vol. 11, no. 2, 2016, PP. 89–94.

[26] Priyadarshini. M., Behera. A , Biswas. C. K., & Rajak. D. K., "*Experimental Analysis and Mechanical Characterization of AISI P20 Tool Steel Through Heat-Treatment Process*," J. Bio-Tribo-Corrosion, Vol. 8, no. 1, 2022, PP. 3-13.

[27] Mohanty. R. K., Mohanty. R. C., & Sabut. S. K., "*Finite element analysis and experimental validation of polycentric prosthetic knee*," Mater. Today Proc., vol. 63, pp. 207–214, 2022, doi: 10.1016/j.matpr.2022.02.509.